Statistical characterization of simulated annealing applied to the x-ray phase problem

Michael F. Zimmer and Wu-Pei Su
Department of Physics and Texas Center for Superconductivity, University of Houston, Houston, Texas 77204
(Received 13 May 1998)

This paper examines the statistical behaviors of variables in the simulated annealing (SA) algorithm when it is used to solve the x-ray phase problem. The results found help remove ambiguities of its application, and clarify its analogy to statistical mechanics. The x-ray phase problem consists in discovering unknown atomic positions of a crystal, given its x-ray diffraction data. SA solves this problem by selectively accepting random trial atomic positions; a cost function is used to measure the nearness of the experimental structure factor to that from a trial solution. The algorithm treats a cost function as an (artificial) energy, a control parameter as a (artificial) temperature, and recovers an optimal solution by lowering the temperature through a cooling schedule. In this paper the probability distribution of the energy is numerically calculated, and provides the first two moments of the energy versus temperature; an approximate solution is also provided. This result shows that the sudden drop in energy often seen in SA runs is actually a transition to a nonequilibrium state. The average configuration error for a given energy is determined, and provides a measure of the quality of a solution. Analytic estimates are made of the high-temperature behavior, which are of use in determining the cooling schedule. Finally, the dependence of the normalization factor for the data is calculated and shown to mirror the solution quality. These results are applied to an ideal crystal with orthorhombic symmetry, and also to real data on the $C_{18}H_{22}O_2$ molecule (with $P2_1/c$ symmetry). [S1063-651X(98)14210-1]

PACS number(s): 02.70.Lq, 61.43.Bn, 42.30.Rx, 64.90.+b

I. INTRODUCTION

The x-ray phase problem consists in determining the atomic positions of an unknown crystal, given its x-ray diffraction data and perhaps other information on the crystal structure. The ability to solve for unknown structures is of great practical importance. For example, the discovery of new proteins could help significantly in the design of new drugs, perhaps for fighting cancer. It has been demonstrated [1] that this problem is amenable to the simulated annealing (SA) algorithm developed by Kirkpatrick *et al.* [2]. The method centers around a suitably defined cost function (or energy) that defines the nearness to a target solution. In this case, the energy essentially measures the difference between the experimentally determined structure factor and that derived from a trial configuration of the atoms. A Monte Carlo algorithm [3] is used to search these trial configurations, where the role of the temperature is taken over by a control parameter. The temperature is lowered according to a cooling schedule, forcing the system to explore lower-energy configurations; in this way an optimal solution is found. Another technique that has been successful on the phase problem is the direct method; this approach is reviewed by Woolfson [4].

The purpose of this paper is to discover how the simulated annealing algorithm works in this application, so that it may be better applied to the x-ray phase problem. One would expect that results found here would carry over to some of its myriad applications; examples include very large scale integrated (VLSI) chip design [2,5], the traveling-salesman problem [2,6], spin-glass ground states [7], image analysis [8,9] and pattern recognition [10], graph partitioning [11], code generation [12], least-squares fitting of many unknowns [13], etc. In general, such a stochastic approach is efficient in situations where it is (practically) impossible to search every configuration, or where traditional methods fail, perhaps because of a large number of local minima in the cost function. It should be pointed out that beyond the original formulation [2], works of a theoretical nature are few and scattered. For example, work on cooling schedules has produced a proof that at sufficiently slow cooling, the exact solution will be found with probability one [8,14]. Heuristical cooling schedules offer improvements when resources are limited, but no general picture has been painted to say which is best. There have also been configuration space analyses that found evidence for hierarchical statistics [15]. Also, the phase transition behavior of certain models has been studied with the application of the so-called replica trick [16]. While these results are important in their own right, they do not directly bear on clarifying matters in the application of SA to the phase problem. For example, one would like to know what is going on when the energy drops suddenly, in a manner reminiscent of a phase transition. It is not known: if this is an analog of a phase transition; if it is a nonequilibrium effect; if it strongly affects the quality of the final solution; if it would be better to try to avoid it, or even if it is avoidable. In short, *any information* that can be used to help understand or predict the SA algorithm is of practical use and should be pursued, especially when one considers how wide-ranging the applications are.

A number of results are presented here, most important of which is the determination of the probability distribution of the energy. This allows the average energy and its variance to be determined as a function of temperature. To the authors' knowledge, this has not been done on any problem studied with SA. In this case, it allows us to show that the apparent phase transition is a nonequilibrium effect, due to the system getting stuck in a low-energy configuration. This happens at the same point as the vanishing of the acceptance ratio. In addition to determining the energy distribution by

convolution, a quick prescription is also given for its approximation. In the limit of high-temperature sampling, accurate estimates are made of the energy and its variance. In addition to giving information for the initial temperature, they also provide a means for quickly estimating the normalization factor between the structure factor from experiment and theory. The temperature dependence of this normalization is found to mirror the accuracy of the solution. Finally, it is demonstrated how this accuracy can be computed as a function of energy. The above techniques are introduced and tested on an ideal crystal with orthorhombic symmetry in Sec. III. Many of them are reapplied in Sec. IV, for a real crystal with $P2_1/c$ symmetry.

II. THE X-RAY PHASE PROBLEM AND SIMULATED ANNEALING

The phase problem consists in determining the atomic positions of an unknown crystal given its structure factor data. Other information such as the number and types of the constituent atoms may or may not be available. The structure factor F, which is the Fourier transform of the electron density (ρ),

$$F(\vec{k}) = \int d^3\vec{r}\,\rho(r)e^{i\vec{k}\cdot\vec{r}}, \tag{1}$$

is measured at a number M of reflections (or k points), where $\vec{k}$ is a reciprocal lattice vector for the given crystal group; the position vector $\vec{r}$ is integrated over the unit cell. However, because the intensity $\propto|F|^2$ does not contain phase information and because M is always finite, it is not possible to exactly invert the transform and determine the unknown ρ.

As mentioned in the Introduction, there are a number of approaches that have been taken to overcome this lack of information. The one studied here is the SA algorithm, which seeks the solution by stochastically searching the space of available configurations. At the heart of the algorithm is the cost function, or energy, which measures the goodness of fit (or quality of the solution). For this problem it may be defined as

$$E = \sum_{\{k\}} E_k \equiv \frac{1}{M}\sum_{\{k\}} \{|F_d(\vec{k})| - \lambda|F_t(\vec{k})|\}^2 \tag{2}$$

so that $E=0$ corresponds to the exact solution (λ is a normalization parameter); other qualitatively similar forms for E will be considered in a later section. Here, $|F_d|$ is the magnitude of the structure factor as measured in experiment, and $|F_t|$ is the computed version, based on a trial configuration. It may appear that this could be straightforwardly solved by steepest descent or a related technique, but there is a serious difficulty in that there are multiple minima in the function $E(\{\vec{r}\})$ (where $\{\vec{r}\}$ is the set of positions of the atoms). These minima can be shown using an $F_d(\vec{k})$ (with $M=126$) calculated from an artificial two-dimensional circular molecule comprised of eight atoms. For example, in Fig. 1(a) is shown a trial configuration for this molecule, in which all the atoms are in the correct position, except for the one that is allowed to move along a line. The energy for the system as a function of this movable atom is given in Fig. 1(b). Aside from the lowest point corresponding to the correct position of the free atom (as it should), the most notable feature is the presence of multiple minima. The smallest scale in this graph should scale with the inverse of the maximum $|\vec{k}|$ in the data set.

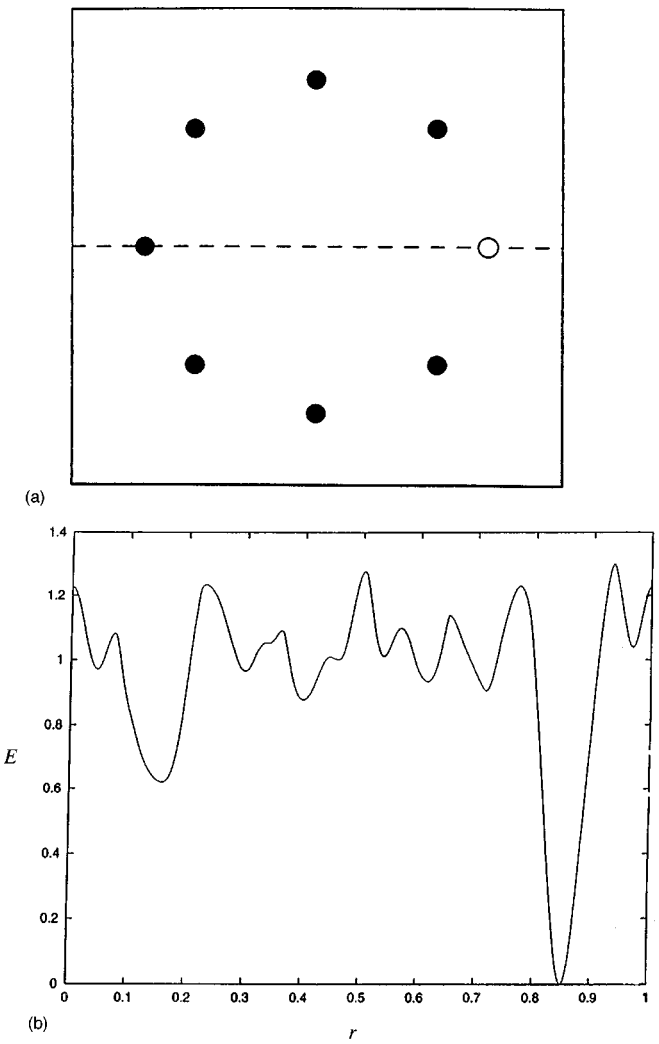

FIG. 1. The positions of the data atoms are indicated by the eight circles. Seven of the trial atoms are fixed in the correct positions (filled circles); the eighth atom (unfilled circle) is allowed to move along the dashed line. (b) The energy as a function of position as the free atom moves along this line.

The SA algorithm was designed to avoid these metastable minima by occasionally allowing the search to move uphill in energy. The algorithm is based on an analogy to statistical mechanics, in which each configuration of the system (i.e., arrangement of the atoms) is assigned a Boltzmann probability $\exp[-E(\{\vec{r}\})/T]$, where T is normally the temperature, but is here just a control parameter (the Boltzmann constant is set to one throughout this paper). This distribution is recovered by Monte Carlo sampling. For example, using the Metropolis scheme, an update from an energy E to $E+\Delta E$ is accepted if

$$\mu \leqslant \min[1, \exp(-\Delta E/T)], \tag{3}$$

where μ is a random number on the unit interval. If the sampling is ergodic, the updating will sample configurations with a Boltzmann weight. Upon lowering T (according to

some cooling schedule), the Boltzmann weight $e^{-E/T}$ favors lower-energy configurations, and thus improves the quality of the solution. An obvious advantage this technique has over steepest descent, for example, is that higher energies may be explored, and thus becoming trapped in a local minimum is less serious of a danger. In addition, the parameter λ will be perturbed (as the energy was), and new values will be accepted according to the same Metropolis criterion.

III. IDEAL CRYSTAL

In this section the relatively simple case of a crystal with orthorhombic symmetry, no internal symmetry, and pointlike atoms will be used to demonstrate certain statistical techniques. The atoms will be modeled with δ functions, making the atomic structure factor equal to one. This is actually very similar to the case where all atoms are of the same type, since then it can be written as a single prefactor in the structure factor. Also, without loss of generality, the sides of the unit cell are set to unit length. The positions of the $N=10$ data atoms are generated randomly. The reciprocal lattice vectors are

$$\vec{k}=2\pi(m_1,m_2,m_3), \tag{4}$$

where each m is an integer, and $\vec{k}=\vec{0}$ is excluded. The set of k points used form a sphere in k space with one half removed, in order to account for the degeneracy in the structure factor when $\vec{k}\rightarrow-\vec{k}$. Also, since the data are generated in a program, its normalization is known and λ may be set to one. Later, a prescription will be given for estimating it in a general scenario. Finally, no thermal effects will be considered.

Summarizing the situation, there are M k points, at which the data $F_d(\vec{k})$ is generated, which represents the square root of the intensity in an x-ray diffraction experiment. The SA algorithm involves many trial guesses of the positions of the data atoms, which are used to calculate the magnitude of the trial structure factor F_t:

$$F_t(\vec{k})=\sum_{j=1}^{N} e^{i\theta_j}, \tag{5}$$

where $\theta_j=\vec{k}\cdot\vec{r}_j$. In this scenario where the $\vec{r}_j$ are generated randomly, it can be shown (see Appendix A) that θ_j may be taken as uniformly distributed on $(0,2\pi)$, so long as it is used in a 2π-periodic function (as is done here). Thus $|F_t|$ represents the magnitude of a sum of complex numbers, each pointing in a random direction, and each of unit length. Clearly, the distribution for F_t is the same as that of an N-step two-dimensional random walk [17]. The distribution for the magnitude of F_t is just

$$P_r(|F_t|)=\frac{2|F_t|}{N}\exp(-|F_t|^2/N). \tag{6}$$

This has been compared to that resulting from a histogram of $|F_t|$, made by randomly generating the phases θ. The agreement was quite good, but slight differences were noticeable. Finally, it is pointed out that the distribution of the $|F_d|$ should also be given by the above equation, since the data were formed in the same way. Each is plotted in Fig. 2 to demonstrate the fact.

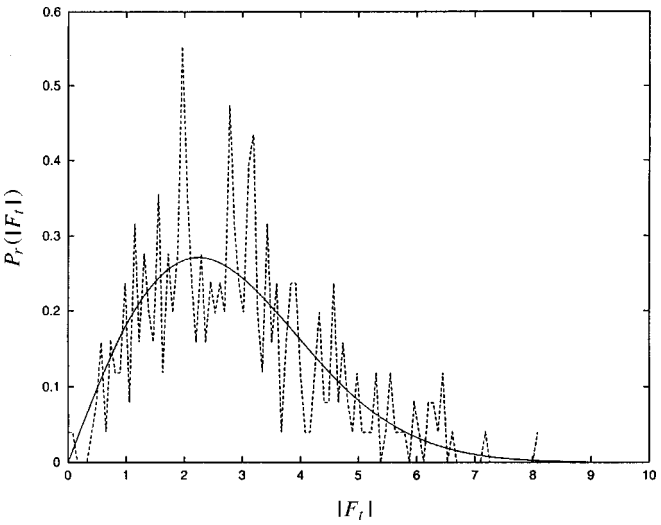

FIG. 2. Plot of $P_r(|F_t|)$ (smooth line) as determined from the CLT and a histogram of $|F_d|$ (jagged line). Since the data F_d are described by the same distribution, it follows the same curve as for $P_r(|F_t|)$.

A. Determination of $P_r(E_k)$

As stated earlier, the goal is to determine the probability distribution of E. Toward that end, it was necessary first to find the distribution of $|F_t|$, and now to find the distribution of $E_k=(1/M)\{|F_d(\vec{k})|-|F_t(\vec{k})|\}^2$. Formally, the probability distribution for E_k can be written as

$$P_r(E_k)=\int_0^\infty d|F_t|\,\delta[E_k-\{|F_d(\vec{k})|-|F_t(\vec{k})|\}^2/M]P_r(|F_t|), \tag{7}$$

where $P_r(\cdot)$ is used to denote the probability distribution of $(\cdot)$. This expression may look somewhat unapproachable, but it is easily implemented numerically by going through allowed values of $|F_t|$, calculating $\{|F_d|-|F_t|\}^2/M$, and incrementing the bin for $P_r(E_k)$ by the value $P_r(|F_t|)d|F_t|$. A representative plot of $P_r(E_k)$ for the sample values $F_d=4.0$ and $M=310$ is shown in Fig. 3.

As will become apparent in the following section, it is very important to know if there exist any correlations among the E_k. Toward determining this, it is helpful to recall the algorithm that leads to values for the E_k. In a simulation, $3N$ random numbers are generated for $F_t(\vec{k})$. For any given $\vec{k}$, the N (complex) terms in each $F_t(\vec{k})$ are of course independent, but it is less clear that the θ_j are. They are, however, related as $\theta_j=\theta_j'+(\vec{k}-\vec{k}')\cdot\vec{r}_j$. Hence, so long as $\vec{k}\neq\vec{k}'$, the $(\vec{k}-\vec{k}')\cdot\vec{r}_j$ term will produce a random number uniformly distributed on $(0,2\pi)$. Thus each of the NM different $\theta_j(\vec{k})$ will act as an independently distributed random number. It follows that each $F_t(\vec{k})$ will be made up of its own N (complex) random numbers. Since the $F_t(\vec{k})$ are independent, so will be the E_k, and hence there is no correlation among them. Finally, it is pointed out that while this argument goes

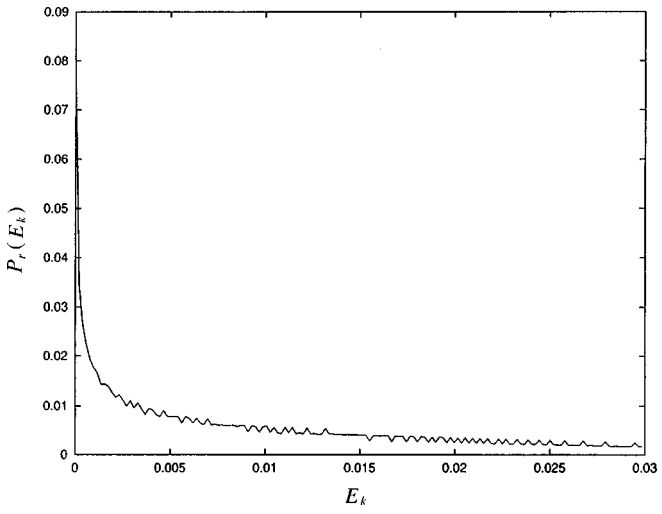

FIG. 3. A representative plot of $P_r(E_k)$ for the sample values $F_d=3.0,\ M=310,\ N=10$.

through smoothly for crystals of orthorhombic symmetry, it requires amendments for other symmetries, such as the $P2_1/c$, which will be discussed in the second half of the paper.

B. Determination of $P_r(E)$

Because the E_k are independent, determining the distribution of E by convolution is very much simplified. In this case, the distributions for the E_k may be convoluted two at a time. This approach works well when there are no more than a few hundred k points, but for any more, errors start building up in the several percent range. To deter this effect, it was found that convoluting the set of k points in batches of 50, for example, and then later convoluting these batches, would reduce the errors in the mean and variance back within the 1% range. The results for the energy and variance are plotted in Figs. 4(a) and 4(b) for several different $\{\vec{k}\}$ sets ($M=153,310,511$) with N fixed at 10; the averages were of course computed using the partition function

$$Z(T)\sim\sum_E P_r(E)e^{-E/T}. \tag{8}$$

It was observed that for large M the energy curve made sharper drops, as it approached zero. These will serve as a basis of comparison to the SA runs in Sec. III C.

An approximate distribution for E may also be calculated, by making use of a variation of the usual central limit theorem (CLT). The reason this variation is called for is because the distribution for each E_k is slightly different, owing to the different F_d that they depend on [see Eq. (2)]. In Appendix B it is shown that the conditions necessary for this more general CLT are indeed met, and so the usual Gaussian distribution may be used to describe E. The final necessary input is the mean μ_E and variance σ_E of the energy. This may be found by summing the means and variances of the individual E_k, or alternatively (and more quickly) by just measuring them while randomly sampling the trial atomic positions (equivalent to a high-temperature measurement in SA). Through either approach, the resultant distribution is just

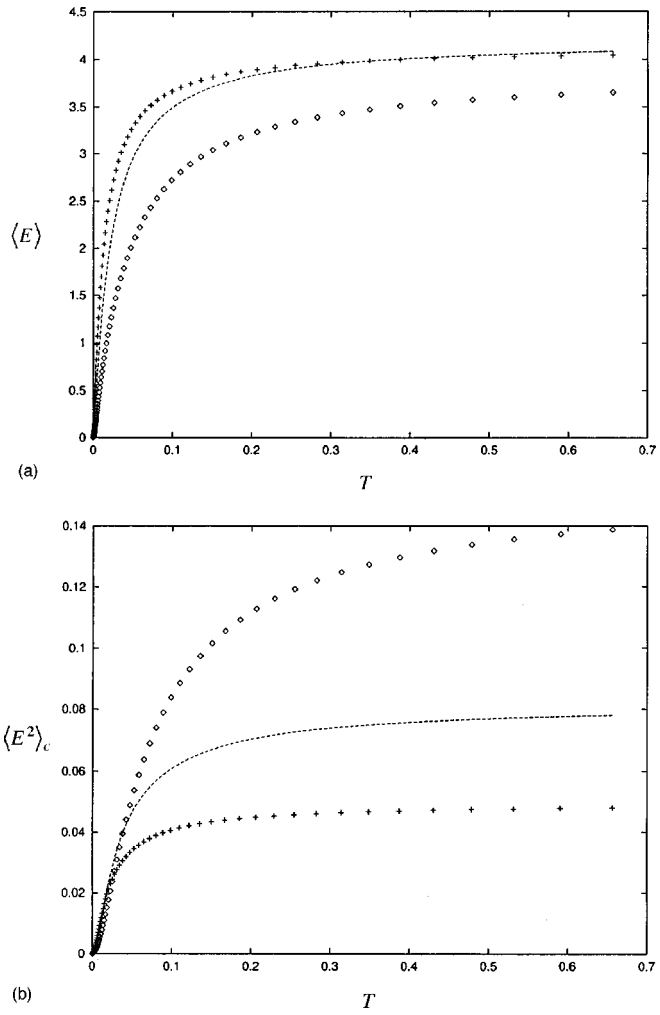

FIG. 4. (a) Plots of $\langle E\rangle$ as found by convolution for $N=10$ and $M=153$ (lower dots), 310 (line), and 511 (upper dots); these demonstrate the sharpening dropoff as M increases. (b) Plots of $\langle E^2\rangle_c$ as found by convolution for $N=10$ and $M=153$ (lower dots), 310 (line), and 511 (upper dots).

$$P_r(E)\sim\exp\left\{-\frac{(E-\mu_E)^2}{2\sigma_E^2}\right\}. \tag{9}$$

Finally, it will be noted that this CLT approximation is only reasonable for energies $\sim\mu_E\pm\sigma_E$.

There are thus two means of determining $P_r(E)$ at our disposal: the convolution approach, which is more difficult, but gives an accurate answer; and the CLT approach, which is very quick, but is only reasonable for deviations of roughly one standard deviation. For comparison, the two distributions are plotted together in Fig. 5. They are quite similar, and it takes a discerning eye to note that the convolution result is slightly skewed to the right, favoring higher energies. Perhaps more instructive is to see what they predict for certain averages. In Fig. 6(a) is $\langle E\rangle$ for $M=310,\ N=10$ as found by convolution and through the CLT. This is typical plot, with the result from convolution always giving a higher value than that from the CLT; this follows from the aforementioned skewness. In Fig. 6(b) is $\langle E^2\rangle_c$ for the same data, with the result from the CLT showing a conspicuously flat

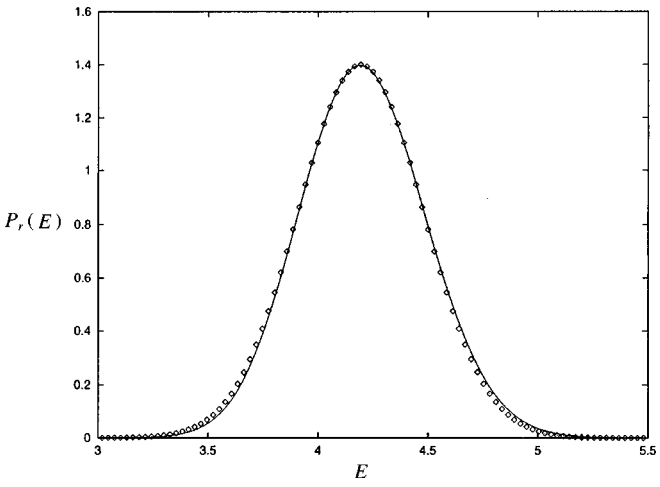

FIG. 5. Plot of $P_r(E)$ from convolution (line) and CLT (dots), using $N=10$, $M=310$. By construction, they have the same mean and variance.

distribution. (Note that the CLT results could also have been written in terms of error functions.)

On a final note, it is pointed out that $P_r(E)$ is proportional to the number of states with that energy. The missing normalization factor is the just the total number of allowed states. To calculate this it is necessary first to regularize (i.e., discretize) the allowed atomic positions in the unit cell to V total sites. The number of positions for N distinguishable atoms on a lattice with V positions (with $V \gg N$) is $V!/(V-N)! \sim V^N$, when multiple occupations are not allowed. Including this normalization factor, the total number of states is then just $e^{-S(E)} \sim V^N P_r(E)$, where $S(E)$ is the usual entropy.

C. Simulated annealing results

The results of the above section are here compared to SA runs; the same data will be used with $N=10$, $M=310$. In Fig. 7(a) the average energy is plotted along with the result found by convolution [already shown in Fig. 4(a)]. Of note is the closeness of the two plots for high energies, which continues down to $T \approx 0.05$. This temperature is significant since it is close to where the acceptance ratio is near zero, as shown in Fig. 7(c). It is at this point that there is a sudden drop in the energy in the SA approach, and has been likened to a phase transition by some authors. What appears to be happening is that near that temperature the acceptance ratio is so low that once it finds a low energy, it does not have enough opportunities to escape to a higher energy to ever recover. Thus it is not able to explore a representative portion of its phase space, and it effectively makes a transition to a nonequilibrium state. In earlier observations of this phenomenon, the origin of the transition was not at all clear. In addition, certain authors (see references within Ref. [14]) have argued for cooling schedule formulas based on equilibrium identities; what was found here is that these formulas lose their basis past this ''phase transition'' point.

The variance also presents some interesting behavior [see Fig. 7(b)]. When calculated via convolution, it shows a smooth decline as the temperature is lowered. However, when measured using SA, it shows pronounced fluctuations

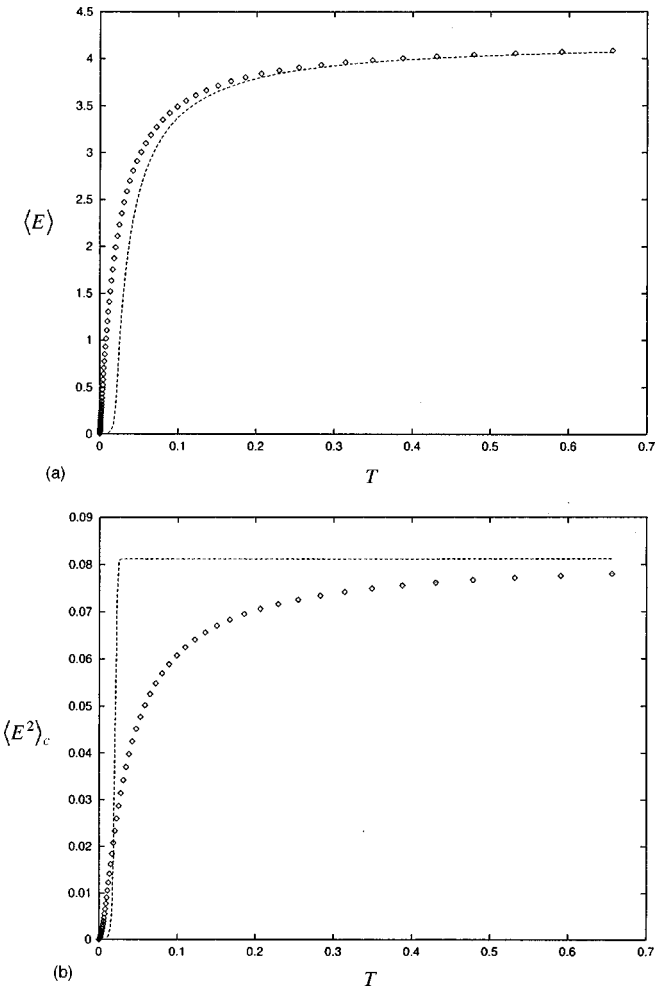

FIG. 6. (a) The average energy for $N=10$, $M=310$ as found by convolution (dots) and through the CLT (line). (b) The variance of the energy for $N=10$, $M=310$ as found by convolution (dots) and through the CLT (line).

near this transition temperature. It is likely the case that there are many measurements of E at equilibrium and in a nonequilibrium state; this could well lead to the large variations seen in $\langle E^2 \rangle_c$. It seems less likely that these variations are due to a susceptibility that is intermittently present.

D. High-temperature limit

In the high-temperature limit, nearly every configuration is accepted in the Metropolis scheme [see Eq. (3)], and so the sampling of an energy is proportional to $P_r(E)$. In the case where $P_r(E)$ is sharply peaked about some characteristic energy (as in this problem), the high-T averages are determined by the behavior of $P_r(E)$ near the peak. In this case, the average energy may be found directly [using Eq. (8)], and the variance may also be easily calculated; complications arise when there are correlations among the E_k (as with other symmetries).

The high-T averages will be found by uniformly averaging over the trial positions, i.e., by averaging with respect to $P_r(E)$. With $\lambda=1$, the limiting average energy is

$$\langle E \rangle = \frac{1}{M} \sum_{\{k\}} \langle E_k \rangle = N + \frac{1}{M} \sum_{\{k\}} [\,|F_d(\vec{k})|^2 - \sqrt{\pi N}|F_d(\vec{k})|\,]. \tag{10}$$

Also, since the E_k are uncorrelated, as shown earlier, it is possible to calculate the variance straightforwardly.

$$\langle E^2\rangle_c = \sum_{\{k,k'\}} \langle E_k E_{k'}\rangle - \frac{1}{M^2}\left(\sum_{\{k\}} \langle E_k\rangle\right)^2 = \sum_{\{k\}} \langle E_k^2\rangle - \langle E_k\rangle^2$$
$$= \frac{1}{M^2}\left\{ N(4-\pi)\sum_{\{k\}} F_d(\vec{k})^2 - N\sqrt{\pi N}\sum_{\{k\}} |F_d(\vec{k})| + MN^2\right\}. \quad (11)$$

For the case of $N=10$, $M=310$, the above formulas produce the values $\langle E\rangle \approx 4.30$ and $\langle E^2\rangle_c \approx 0.0905$. These numbers should be compared with $4.19\ldots$ and $0.0801\ldots$, respectively, which were obtained from a SA run at high temperature. The agreement improves quickly for larger N. For example, for $N=20$ the error in the energy is close to 1%. Furthermore, these may be averaged over with respect to F_d, to obtain results for an average crystal of this symmetry. For example, in this case $\langle E\rangle = (2-\pi/2)N$. Finally, the results may be easily extended to other cost functions [18] besides Eq. (2) (but with the same crystal symmetry). For example, those of the form $(|F_d|^p - |F_t|^p)^q$ (p,q integers; $p>0$, $q>1$) may be readily found.

E. Accuracy of the solution

As the temperature is lowered and the energy decreases, it may be reasonable to write the data and trial structure factors as

$$F_d(\vec{k}) = \sum_{j=1}^{N} e^{i\vec{k}\cdot\vec{r}_j}, \quad F_t(\vec{k}) = \sum_{j=1}^{N} e^{i\vec{k}\cdot(\vec{r}+\vec{\Delta r})_j}, \quad (12)$$

where $\vec{\Delta r}$ is a random deviation. It is a practical idealization to think of the trial position as hovering about the correct position of a data atom. Indeed, for any given run, it may be the case that several atoms lie where a single one should, or that they bear some incorrect but symmetrical arrangement to where the atoms should be. These special situations are expected to be subsumed in the following averaging procedure.

The fluctuation of the position of the jth atom is modeled by a Gaussian distribution with standard deviation σ:

$$P_r(\vec{\Delta r}_j) = \frac{1}{\sigma\sqrt{2\pi}}\exp\left\{-\frac{1}{2}\left(\frac{\vec{\Delta r}_j}{\sigma}\right)^2\right\}. \quad (13)$$

In this section an average input crystal will be studied, meaning that each $\vec{r}_j$ will be uniformly averaged over the unit cell. Using angular brackets to denote the averages over $\vec{r}$ and $\vec{\Delta r}$, the energy [Eq. (2)] becomes

$$\langle E\rangle = \frac{1}{M}\sum_{\{k\}} \{2N - 2\langle |F_d||F_t|\rangle\} \quad (14)$$

since for any value of $\vec{k}$ and σ, $\langle |F_d|^2\rangle = \langle |F_t|^2\rangle = N$. The problem has thus become one of determining the correlation $\langle |F_d||F_t|\rangle$, and will be pursued numerically. Since the $\vec{r}_j$ are sampled randomly, $\vec{k}\cdot\vec{r}_j$ is uniformly distributed on $(0,2\pi)$. Also, the distribution of $\eta = \vec{k}\cdot\vec{\Delta r}$ [i.e., $P_r(\eta)$] is simply a zero-mean normal distribution with standard deviation $\gamma = \sigma|k|$. Thus the goal now is to calculate

$$\epsilon(\gamma) = 2N - 2\langle |F_d||F_t|\rangle_{r,\eta} \quad (15)$$

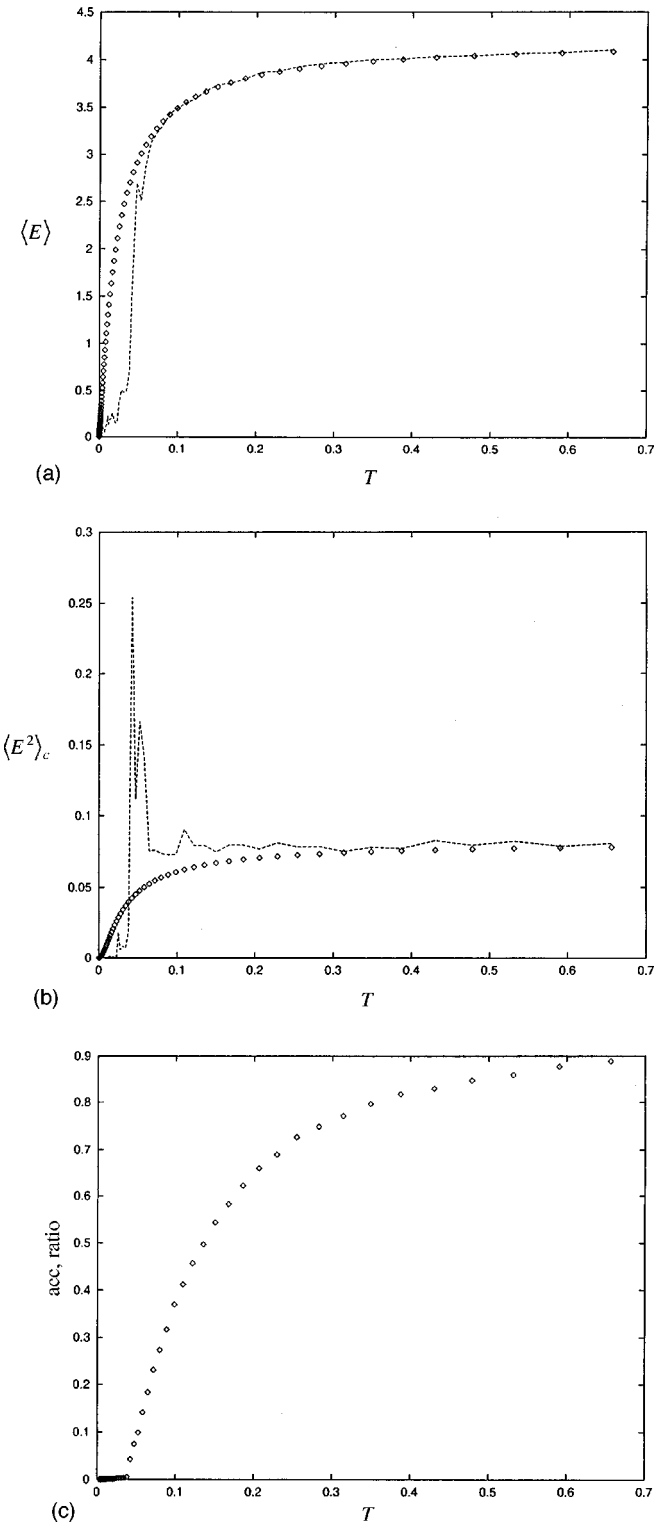

FIG. 7. (a) Average energy by convolution (line) and by SA (dots). (b) Variance by convolution (line) and by SA (dots). (c) Acceptance ratio in the SA run.

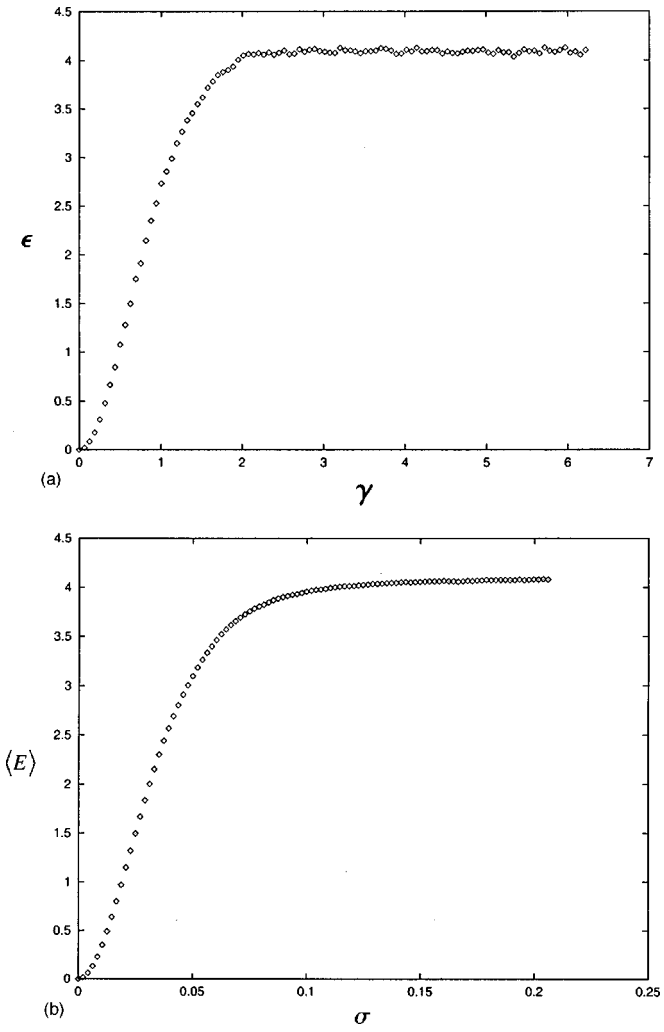

FIG. 8. (a) $\epsilon(\gamma)$ for an ideal orthorhombic crystal with $N=10$ atoms. (b) $E(\sigma)$ for $N=10$ and $M=310$.

by sampling $\vec{k}\cdot\vec{r}$ from $(0,2\pi)$ and using $P_r(\eta)$ to sample η. This was done for $N=10$, $M=310$ and the result is displayed in Fig. 8(a). Due to the sharp dropoff of this curve for $\gamma\approx 1.0$, it is clear that $|F_d(\vec{k})|$ and $|F_t(\vec{k})|$ can remain correlated only up to $\sigma\approx|\vec{k}|^{-1}$. Finally we note that $\epsilon(\gamma)$ displays the expected limiting behavior:

$$\epsilon(\gamma\rightarrow\infty)=(2-\pi/2)N, \tag{16}$$

$$\epsilon(\gamma=0)=0. \tag{17}$$

Now that this has been determined, all that is necessary to calculate $E(\sigma)$ is a data set $\{k\}$. Using the same set as for $M=310$ (see Fig. 7), the relation

$$E(\sigma)=\frac{1}{M}\sum_{\{k\}}\epsilon(\sigma|\vec{k}|) \tag{18}$$

leads to the result shown in Fig. 8(b). This is very interesting because it shows that once the energy begins to drop, the positions are already quite localized. For example, in Fig. 7(a) for $M=310$, when $\langle E\rangle$ is about half its plateau value, $\sigma\approx 0.02$; here the positions are localized to within about $\pm 2\%$ of their correct values (measured with respect to a side of a unit cell). This curve was also computed for $M=153$ and 511 and showed only minor differences, although it tended to become steeper for larger M. To the authors' knowledge, this is the only time an estimate of the error as a function of temperature has been given in a simulated annealing application. Finally, we note that this situation is analogous to crystalline melting, as explained by the Lindemann criterion. There it is also the case that the gradual increase in the atomic deviations leads to a sudden drop in the coherence.

F. Determination of λ

As mentioned earlier, the parameter λ is updated stochastically [1,19], with the new value being accepted according to a Metropolis scheme. This kind of approach is necessary, since its value cannot be known beforehand. An alternative would be to average $\langle\partial E/\partial\lambda\rangle=0$ with respect to $P_r(|F_t|)$. For the case of orthorhombic symmetry, the result is easily seen to be

$$\lambda=\frac{1}{2M}\sqrt{\frac{\pi}{N}}\sum_{\{k\}}|F_d(\vec{k})|, \tag{19}$$

which for an average crystal becomes $\lambda=\pi/4$ (N.B.: the average over $|F_d|$ is the same as that over $|F_t|$). It is significant that this does not coincide with the known correct value of $\lambda=1$. This discrepancy is due to ignoring correlations between $|F_d|$ and $|F_t|$, such as were discussed in the preceding section [cf. Eq. (12)]. Upon allowing for such correlations, the value for λ valid for all temperatures is

$$\lambda=\frac{\sum_{\{k\}}\langle|F_d||F_t|\rangle}{\sum_{\{k\}}\langle F_t^2\rangle} \tag{20}$$

and is easily checked [using Eq. (6)] to interpolate between the high-T result of $\lambda=\pi/4$ and the low-T result of $\lambda=1$. As the temperature is lowered, the increased correlation between $|F_d|$ and $|F_t|$ appears in the increased value of λ.

In Sec. III B where $\langle E(T)\rangle$ was found by convolution and by approximation, only a single value of $\lambda=1$ was used. Hence, in a simulation where λ is updated stochastically (as is always the case with real data), those graphs cannot be used for comparison. To properly predict the equilibrium behavior in this scenario, one would need to know $P_r(E)$ for all λ used between $\pi/4$ and 1. As it turns out [18], the only significant difference between the $\langle E(T)\rangle$ found by convolution using different λ is that the overall scale of the graph is changed at high temperatures; this would easily follow from a generalization of the results in the preceding section. More interesting is the behavior of $\lambda(T)$ in a SA run in which λ is updated. Again using $N=10$ and $M=310$, the result is shown in Fig. 9(a). To gauge the location of the transition, $\langle E\rangle$ from the same SA run is plotted in Fig. 9(b), along with the convolution results for the energy for $\lambda=1,\pi/4$; as expected the SA result coincides with the $\lambda=\pi/4$ result for high T. These results vindicate Eq. (20), since it shows that when the energy drops, λ increases, which means that correlations between $|F_d|$ and $|F_t|$ increase; it seems to be slow

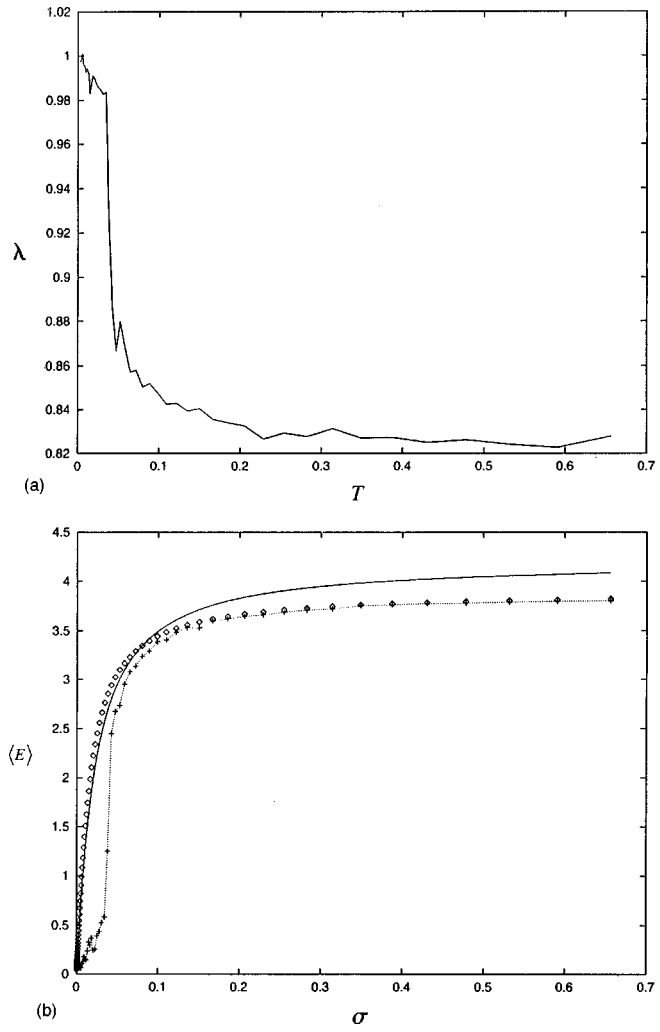

FIG. 9. (a) $\lambda(T)$ for $N=10$, $M=310$; the increase at low T marks an increase of the correlation of $\langle|F_d||F_t|\rangle$. (b) $E(\sigma)$ as generated by convolution for $\lambda=1$ (line), $\lambda=\pi/4$ (dots), overlaid with the result from SA where λ was updated (line marked with $+$). In all cases $N=10$, $M=310$.

in converging to its correct value of $\lambda=1$. This is logical, and is also consistent with the decrease of ϵ for small γ, i.e., large $\langle|F_d||F_t|\rangle$. Thus the increase of λ appears to be a necessary condition for a solution to be found. Finally, we note that the convergence of λ to its correct value of 1 happens only for very small temperature. This slowness most likely also occurs with the real data, and is presumably the cause for the different scalings of $|F_d|$ [see Sec. IV and Eq. (33)].

IV. THE $C_{18}H_{22}O_2$ MOLECULE

In this section the molecule $C_{18}H_{22}O_2$ will be examined, using some of the techniques introduced earlier. The data, which were supplied by J. D. Korp, have monoclinic structure with $P2_1/c$ symmetry; $a=7.97$ Å, $b=15.29$ Å, and $c=5.84$ Å, with $\beta=92.53°$. The number of k points (or reflections) was $M=1222$. Since the number of formula units per cell is $Z=2$, there are a total of 40 atoms per unit cell, although only $N=10$ are independent. The hydrogen atoms were ignored, and oxygen atoms were modeled as carbon atoms; a refined calculation could treat them as distinct. With

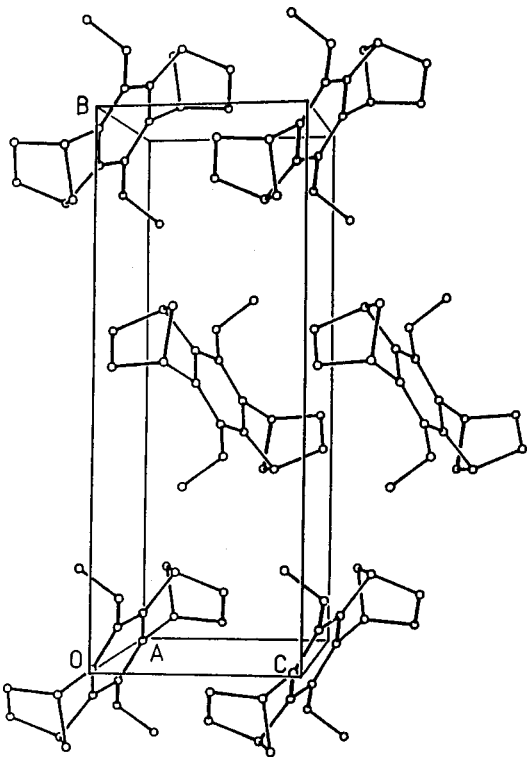

FIG. 10. $C_{18}H_{22}O_2$ in a unit cell, viewed along the a axis.

these data, the structure has been solved by using the SA algorithm [1] (as well as by the direct method [4]). A picture of the molecule is given in Fig. 10. Throughout this section, a simplification was made by taking the sides to be mutually perpendicular; the reciprocal lattice vectors $\vec{k}$ will thus also be given by Eq. (4). The exact calculation only slightly improves the results, but can also be done [18].

The structure factor may be written as

$$F(\vec{k})=\sum_{j=1}^{4N} e^{i\vec{k}\cdot\vec{r}_j}=\sum_{j=1}^{N}\sum_{m=1}^{4} e^{i\theta_m(j)}, \tag{21}$$

where, suppressing the j dependence of the $\theta_m(j)$,

$$\begin{aligned}\theta_1&=\vec{k}\cdot\vec{r}_j,\\ \theta_2&=-\theta_1,\\ \theta_3&=\frac{1}{2}(k_2+k_3)+(-k_1,k_2,-k_3)\cdot\vec{r}_j,\\ \theta_4&=-\theta_3.\end{aligned} \tag{22}$$

A little algebra leads to

$$F(\vec{k})=4\sum_{j=1}^{N}\cos(\delta+k_2y_j)\cos(-\delta+k_1x_j+k_3z_j), \tag{23}$$

where $\delta=\pi(m_2+m_3)$. The most important feature of this is that $\vec{k}\cdot\vec{r}$ has been split between two cosines. Recall that for the orthorhombic symmetry, for a given selection of trial positions, each term in the sum for $F_t(\vec{k})$ was independent not only from all other terms in the sum, but from all other

terms in all the other $F_t(\vec{k}')$. Following the same train of thought, each $F_t(\vec{k})$ could be approximated via the usual CLT, since the mean and variance of each term in Eq. (23) is finite, and the variance is nonzero.

The situation is different when comparing structure factors with different k. Here we consider $\vec{k}=(k_1,k_2,k_3)$ and $\vec{k}'=(k_1',k_2,k_3')$ with m_2+m_3 even, so that

$$F(\vec{k})=4\sum_{j=1}^{N}\cos(k_2y_j)\cos(k_1x_j+k_3z_j),$$
$$F(\vec{k}')=4\sum_{j=1}^{N}\cos(k_2y_j)\cos(k_1'x_j+k_3'z_j). \tag{24}$$

While all the terms within a given F are independent from each other, they will be correlated with one other term in the other F. This is due to the common $\cos(k_2y_j)$ term. The end result of this like term is that correlations exist between E_k with the same k_2 and different k_1, k_3. To complicate matters, there are also correlations between E_k when the pair (k_1,k_3) is the same, and k_2 differs. To demonstrate the extent of this effect, when it is ignored and $P_r(E)$ is calculated by convolution as before, one finds at high temperature $\langle E\rangle \approx 57.9$ and $\langle E^2\rangle_c \approx 2.04$. On the other hand, a random sampling (i.e., a SA run at very high T) shows $\langle E\rangle \approx 57.5$ and $\langle E^2\rangle_c \approx 2.37$. Because of this discrepancy, and also because our point has already been made regarding the ''phase transition,'' we will not pursue calculating $P_r(E)$ for these data.

The mean and variance found at high temperature will be used to define a Gaussian approximation for $P_r(E)$ [as in Eq. (9)]; the temperature-dependent energy and variance will then be compared to a SA run. There will be 1200 updates (700 updates for the high temperatures) of the entire unit cell before lowering T by a factor of 0.9. In this case λ is stochastically updated. In Fig. 11(a) is the result for $\langle E(T)\rangle$; on the same graph is plotted the Gaussian approximation (using a measurement of the mean and variance at high temperature). Although the minimum energy reached by the SA is still about 14% of the initial energy, it is still quite a good solution (as will be seen in the next section). The dependence of the energy on the average error of the solution will be discussed in the next section. Also, the acceptance ratio as a function of temperature was very similar to that for the ideal case.

In a manner similar to what was done in Eq. (10), the high-temperature limit of the energy can be calculated by recourse to a CLT approximation of the structure factors. Since this is only an average we seek and not a distribution, the correlations between some of the E_k are irrelevant here. The only new complication is that averages of powers $|F_t|$ will have two values, depending on which subclass of $\{k\}$ they belong to. Denoting

$$\theta_a(j)=-\delta+k_1x_j+k_3z_j,$$
$$\theta_b(j)=\delta+k_2y_j, \tag{25}$$

the structure factor is now (again suppressing the j dependence)

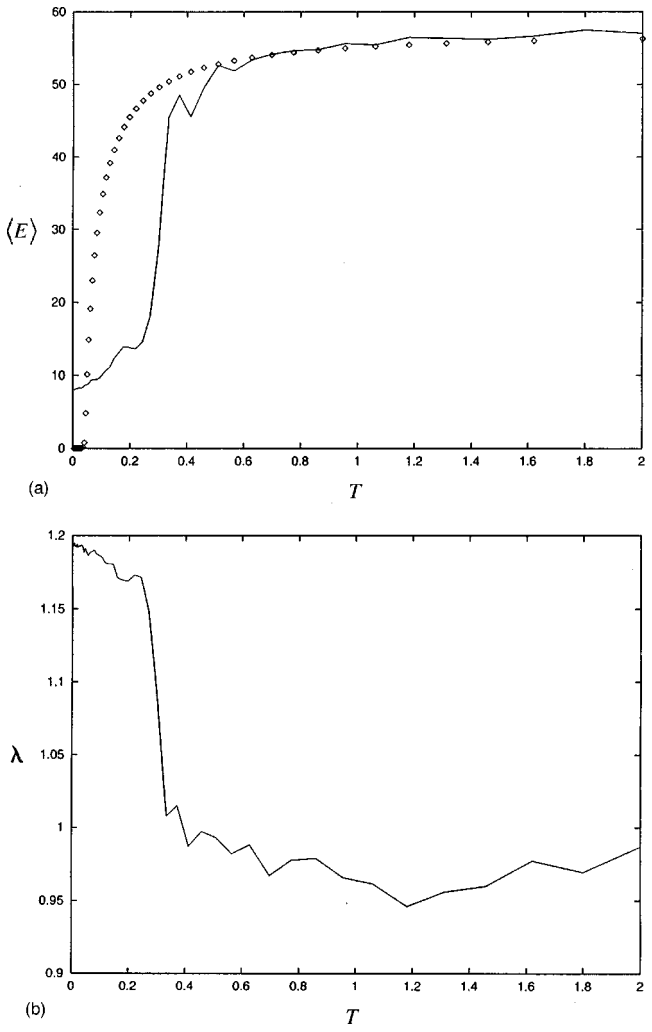

FIG. 11. (a) Plot of $\langle E(T)\rangle$ as found by SA (line) with λ updating, and that generated from a Gaussian fit (dots). (b) Plot of λ versus T, demonstrating the increased correlation between the data and trial atomic positions as T is decreased.

$$F(\vec{k})=4\sum_{j}\cos\theta_a\cos\theta_b. \tag{26}$$

The two cases are the following: (1) both θ_a and $\theta_b\neq 0$; (2) either θ_b or $\theta_a=0$. $F(\vec{k})$ may again be approximated via the CLT, but its specific form depends on the above cases. In case (1) both cosines (or sines) contribute when the mean and variance of each term are calculated. In case (2) only one cosine is present, so the variance is larger. [When m_2+m_3 is odd, only case (1) is present.] Thus, according to the case $i=1,2$, we have

$$\langle|F_t|\rangle=\sigma_i\sqrt{\frac{2N}{\pi}}, \tag{27}$$

$$\langle F_t^2\rangle=\sigma_i^2N, \tag{28}$$

where $\sigma_1=2$ and $\sigma_2=2\sqrt{2}$. When account is made of these two cases and the average energy is calculated via

$$\langle E\rangle=\frac{1}{M}\sum_{\{k\}}\{|F_d|^2-2\lambda|F_d|\langle|F_t|\rangle+\lambda^2\langle|F_t|^2\rangle\} \tag{29}$$

a value of $E \approx 57.8$ is found, which is to be compared to the already mentioned value of 57.5 found from a random sampling measurement (i.e., SA at large T).

Finally, we point out that it is now possible to calculate what λ should be in the high-temperature limit, where $|F_d|$ and $|F_t|$ are totally uncorrelated. Using Eq. (20), we would expect (without scaling $|F_d|$) that $\lambda \approx 0.636$. However, when the real data are used [see Fig. 11(b)], we find $\lambda \approx 0.930$, implying that the scale of $|F_d|$ is about 1.46 times larger than of $|F_t|$. Interestingly, at low temperature SA leads to $\lambda \approx 1.20$, while Eq. (20) gives $\lambda = 1$. As opposed to the ratio of 1.46, these two have a ratio of only 1.20. This serves to support the already clear observation that the true minimum energy has not been reached in the SA run; this may ultimately be due to the limited accuracy of the data $|F_d|$.

Accuracy of the solution

The accuracy of the solution just found by SA can be assessed in a manner similar to that in Sec. III E. However, because the data $|F_d|$ must somehow be taken into account, some approximations must be made. In this case, the data will be used to provide the appropriate overall scale of the energy, so that it may be more easily compared to SA runs. For this approximation F_d will again be related to F_t as in Eq. (12).

Following the presentation of Sec. III E, the positions of the trial atoms will differ from the exact positions by a fluctuation $\vec{\Delta r}$:

$$\theta_a \rightarrow \theta_a + \vec{k}\cdot(\Delta x, 0, \Delta z) \equiv \theta_a + \varphi, \tag{30}$$

$$\theta_b \rightarrow \theta_b + \vec{k}\cdot(0, \Delta y, 0) \equiv \theta_b + \psi. \tag{31}$$

Using the same distribution as in Eq. (13), it follows that φ and ψ are described by zero-mean normal distributions with standard deviations $\alpha = 2\pi\sigma\sqrt{m_1^2 + m_2^2}$ and $\beta = 2\pi\sigma|m_2|$, respectively. As before, because each of the three components of r is uniformly distributed on (0,1), the phases θ_a, θ_b will be uniformly distributed on $(0, 2\pi)$. A simulation that would measure $E(\sigma)$ would thus have to repeatedly draw two random numbers for θ_a and θ_b, and then two more for φ and ψ. As it turns out, a simplifying feature arises because of the identity

$$\langle \cos(\theta_a + \varphi)\cos(\theta_b + \psi)\rangle_{\varphi,\psi} = \exp\{-(\alpha^2 + \beta^2)/2\}\cos\theta_a \cos\theta_b . \tag{32}$$

This allows us to make the approximation that drawing random numbers with the same distributions as for φ and ψ may be replaced by setting $\psi = 0$ in Eq. (32), and using for the distribution of φ, $P_r(\varphi)$, a zero-mean normal distribution with variance $\gamma^2 = \alpha^2 + \beta^2$. The combination $\alpha^2 + \beta^2$ does not occur throughout the second moment in Eq. (32), so this remains an approximation (although it is numerically accurate). It follows then,

$$\epsilon(\gamma) = \left\langle c^2 \left[4\left| \sum_{j=1}^{N} \cos\theta_a \cos\theta_b \right| - 4\left| \sum_{j=1}^{N} \cos(\theta_a + \varphi)\cos\theta_b \right| \right]^2 \right\rangle_{\varphi}$$
$$= 2c^2\langle F_t^2\rangle - 32c^2 \left\langle \left| \sum_{j=1}^{N} \cos\theta_a \cos\theta_b \right| \left| \sum_{j=1}^{N} \cos(\theta_a + \varphi)\cos\theta_b \right| \right\rangle_{\varphi} . \tag{33}$$

The constant $c = 1.46$ is the scaling factor discussed at the end of the preceding section. It is introduced to scale $|F_t|$ to the same size as $|F_d|$, so the energy can be compared to that from SA runs.

Recapitulating, $\epsilon(\gamma)$ can now be calculated by drawing $2N$ random numbers for all of the θ_a and θ_b, with a uniform distribution on $(0, 2\pi)$, and N more for φ with the distribution $P_r(\varphi)$. Repeating this a number of times eventually leads to Fig. 12(a), which is seen to be quite similar in shape to that obtained for the ideal crystal [in Fig. 8(a)]. In conjunction with Eq. (18), the energy as a function of the standard deviation of the positions of the trial atoms can be derived; the result is shown in Fig. 12(b). With this graph it is now possible to assess the errors in position for this data set; there exists no competing method. This is significant since it tells us that once the energy curve begins to drop [in Fig. 11(a)], we can be assured that the error in position, on average, is already within a few percent of the length of the side of the crystal. Also, the sharp drop in $\epsilon(\gamma)$ acts similarly to a Heaviside function, and can be used to relate several characteristic scales. Denoting the average $|\vec{k}|$ by k^*, the σ that would correspond to the median E value would be $\sigma^* = \gamma^*/k^*$. (Thus as more k points are included in $\{k\}$, the smaller σ will be when the energy starts to drop, or go through an apparent phase transition.)

V. CONCLUDING REMARKS

A number of results have been presented for both understanding the algorithm and providing tools to analyze it. It should be emphasized that very little has hitherto existed to do so; most of the results have been of a formal nature, not lending themselves to immediate applicability (with the exception of heuristic cooling schedules).

The apparent ''phase transition'' that regularly appears in the energy versus temperature graphs is now seen to be a consequence of the system falling out of equilibrium, and getting stuck in a portion of its phase space. It is not a consequence of any underlying ''Hamiltonian'' which exhibits phase-transition-like behavior. The expected equilibrium be-

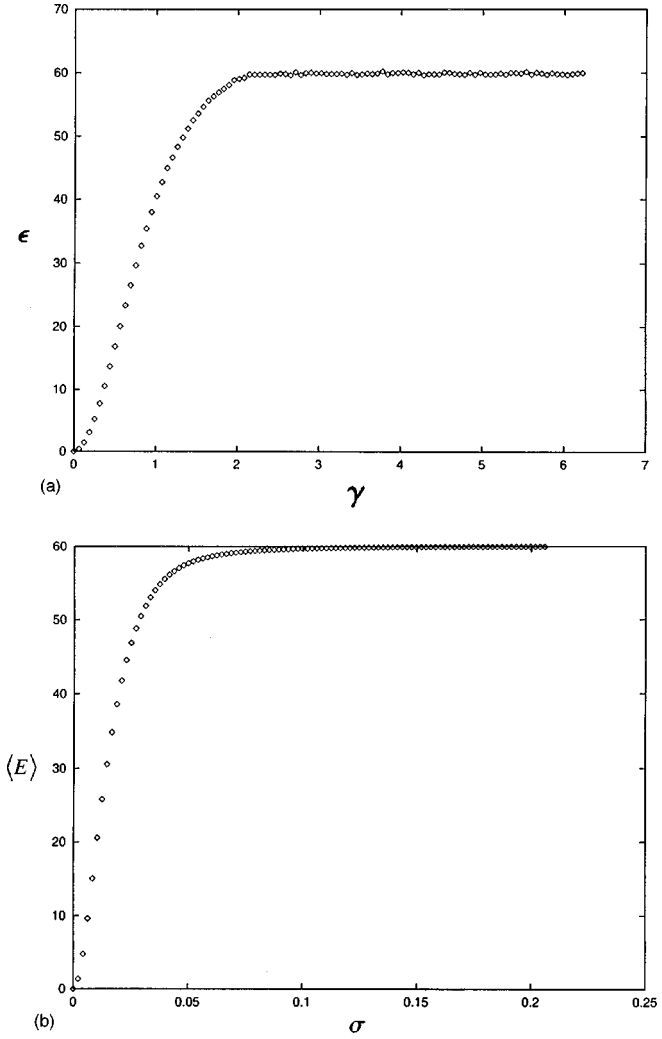

FIG. 12. (a) $\epsilon(\gamma)$ for $C_{18}H_{22}O_2$. (b) $E(\sigma)$ for $C_{18}H_{22}O_2$.

havior can be calculated beforehand by convolution. If the system did not fall out of equilibrium it would follow this path. It can also be calculated in an approximate fashion through a generalized central limit theorem.

Finally, the dependence of the energy on the average standard deviation (between the trial positions and the correct solution) has been calculated for two examples. This provides the user with the valuable information of how close the trial positions are to the real atomic positions.

ACKNOWLEDGMENTS

The authors would like to thank G. Gunaratne and R. Helleman for useful discussions, and J. D. Korp for supplying data on the $C_{18}H_{22}O_2$ molecule. This work was partially supported by the Texas Advanced Research Program under Grant No. 003652-183 and the Robert A. Welch Foundation under Grant No. E-1070. M.F.Z. wishes to express gratitude to the Robert & Charlotte Zimmer Foundation for support under Grant No. 1964.

APPENDIX A

The problem is to find the distribution of $\vec{k}\cdot\vec{r}$ when it is used in the function $e^{i\vec{k}\cdot\vec{r}}$, where $\vec{k}=2\pi(m_1,m_2,m_3)$, each m is an integer, and $\vec{r}=(x_1,x_2,x_3)$, where each x is uniformly distributed on (0,1). First, it is obvious that if f is a 2π-periodic function, then $f(2\pi m_1 x_1+\cdots)=f(2\pi x_1+\cdots)$. Thus, setting $y_i=2\pi x_i$, the problem now is to determine if $y_1+y_2+y_3$ is uniformly distributed when used in f. We shall calculate the distribution of this sum, by convoluting them two at a time (i.e., first $\eta=y_1+y_2$).

Starting from

$$P_r(\eta)=\int_0^{2\pi} dy_1 \int_0^{2\pi} dy_2\, \delta(\eta-(y_1+y_2))P_r(y_1)P_r(y_2) \tag{A1}$$

it is straightforward to show that

$$2\pi P_r(\eta)=\eta\theta(\eta)\theta(2\pi-\eta)+(4\pi-\eta)\theta(4\pi-\eta) \times\theta(\eta-2\pi). \tag{A2}$$

Since η will be used in a 2π-periodic function, the part on $(2\pi,4\pi)$ may be folded over onto $(0,2\pi)$. So when used in this context, $P_r(\eta)=(2\pi)^{-1}$. What has been shown is that, when used in a 2π-periodic function, the distribution of two variables uniformly distributed on $(0,2\pi)$ (i.e., y_1+y_2) produces another variable uniformly distributed on 2π (i.e., η). This leaves us the task yet of finding the distribution of $\eta+y_3$. However, this is the same problem as with y_1+y_2, and we conclude that the distribution of $y_1+y_2+y_3$ (or $k\cdot r$) may be taken as uniformly distributed on $(0,2\pi)$ when used in a 2π-periodic function.

APPENDIX B

In this section a generalization of the usual CLT [20] is discussed, as it requires special conditions for it to hold. It is of use when the terms in the sum (that is being approximated) do not all have the same probability distribution, as with the the sum of E_k [see Eq. (2)].

Let $X_1, X_2, \ldots$ be independent variables satisfying

$$\mathcal{E}X_j=0, \quad \mathrm{var}(X_j)=\sigma_j^2, \quad \mathcal{E}|X_j^3|<\infty \tag{B1}$$

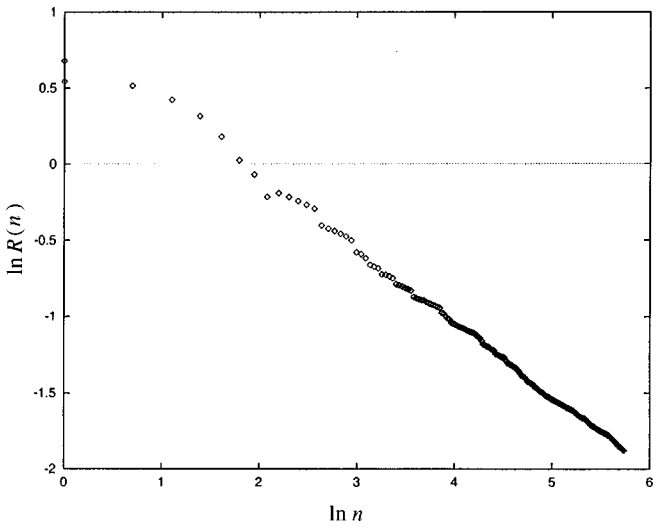

FIG. 13. Plot of ln$R(n)$ versus ln$n$ from Eq. (B2), for the ideal crystal with $M=310$ and $N=10$.

(where $\mathcal{E}$ denotes expectation value) and such that

$$R(n) \equiv \frac{1}{\sigma(n)^3} \sum_{j=1}^{n} \mathcal{E}|X_j^3| \to 0 \quad \text{as} \quad n \to \infty, \tag{B2}$$

where

$$\sigma(n)^2 = \mathrm{var}\left(\sum_{1}^{n} X_j \right) = \sum_{1}^{n} \sigma_j^2 . \tag{B3}$$

Then

$$\frac{1}{\sigma(n)} \sum_{1}^{n} X_j \to N(0,1), \tag{B4}$$

where $N(0,1)$ is a normal distribution with zero mean and unit variance.

In Fig. 13, $\ln R(n)$ is plotted versus $\ln n$ for the case of the ideal crystal with $N=10$, $M=310$, and $n=1,\ldots,M$; n labels the k vectors. This establishes that $R(n)$ vanishes as $n \to \infty$, and thus that this CLT may be used to approximate the sum of the E_k.

[1] S. V. Semenovskaya, K. A. Khachaturyan, and A. G. Khachaturyan, Acta Crystallogr., Sect. A: Crystallogr. **41**, 268 (1985); W.-P. Su, Physica A **221**, 193 (1995); Y.-S. Chen, W.-P. Su, S. P. Mallela, and R. A. Geanangel, Acta Crystallogr., Sect. A: Crystallogr. **53**, 396 (1997).

[2] S. Krikpatrick, C. D. Gelatt, and M. P. Vecchi, Science **220**, 671 (1983).

[3] N. Metropolis, M. Rosenbluth, A. Rosenbluth, A. Teller, and E. Teller, J. Chem. Phys. **21**, 1087 (1953); K. Binder and D. W. Heermann, *Monte Carlo Simulation in Statistical Physics* (Springer-Verlag, Berlin, 1992).

[4] M. M. Woolfson, Acta Crystallogr., Sect. A: Crystallogr. **43**, 593 (1987).

[5] M. P. Vecchi and S. Kirkpatrick, IEEE Trans. Comput.-Aided Des. **CAD-2**, 215 (1983); R. H. J. M. Otten and L. P. P. P. van Ginneken, *The Annealing Algorithm* (Kluwer, Dordrecht, 1989) (contains many references to the literature).

[6] S. Kirkpatrick, J. Stat. Phys. **34**, 975 (1984).

[7] G. S. Grest, C. M. Soukoulis, and K. Levin, Phys. Rev. Lett. **56**, 1148 (1986).

[8] S. Geman and D. Geman, IEEE Trans. Pattern. Anal. Mach. Intell. **PAMI-6**, 721 (1984).

[9] H. L. Tan, S. B. Gelfand, and E. J. Delp, IEEE Trans. Pattern. Anal. Mach. Intell. **14**, 3 (1992); W. E. Smith, R. G. Paxman, and H. H. Barrett, J. Opt. Soc. Am. A **2**, 491 (1985).

[10] G. E. Hinton, T. J. Sejnowski, and D. H. Ackley, Department of Computer Science, Carnegie-Mellon University Report No. CMU-CS-84-119, 1984 (unpublished).

[11] P. Salamon, J. Nulton, J. R. Harland, and J. Pedersen, Comput. Phys. Commun. **49**, 423 (1988).

[12] A. A. El Gamal, L. A. Hemachandra, I. Shperling, and V. K. Wei, IEEE Trans. Inf. Theory **33**, 116 (1987).

[13] D. Vanderbilt and S. G. Louie, J. Comput. Phys. **56**, 259 (1984).

[14] P. J. M. van Laarhoven and E. H. L. Aarts, *Simulated Annealing: Theory and Applications* (Reidel, Dordrecht, 1987).

[15] S. Kirkpatrick and G. Toulouse, J. Phys. (Paris) **46**, 1277 (1985); S. A. Solla, G. B. Sorkin, and S. R. White, in *Disordered Systems and Biological Organization*, edited by E. Bienenstock *et al.* (Springer-Verlag, Berlin, 1986).

[16] M. Mézard and G. Parisi, Phys. Rev. Lett. **52**, 1156 (1984); J. Phys. (Paris) **47**, 1285 (1987); Y. Fu and P. W. Anderson, J. Phys. A **19**, 1605 (1986).

[17] After rediscovering this analogy, we found the first mention of it: K. Pearson, Nature (London) **72**, 294 (1905).

[18] M. F. Zimmer (unpublished).

[19] W.-P. Su, Acta Crystallogr., Sect. A: Crystallogr. **51**, 845 (1995).

[20] G. R. Grimmett and D. R. Stirzaker, *Probability and Random Processes* (Oxford University, New York, 1992).